scientific reports

Check for updates

OPEN

Itinerant-localized dichotomy in magnetic anisotropic properties of U-based ferromagnets

Alexander B. Shick[1,2,3]✉, Itzhak Halevy[4], Maxim Tchaplianka[1] & Dominik Legut[3]

The electronic structure, spin and orbital magnetic moments, and the magnetic anisotropy energy in selected U-based compounds are investigated making use of the correlated band theory. First, we demonstrate that the LSDA+U approach with exact atomic limit implemented as a combination of the relativistic density functional theory with the Anderson impurity model provides a good quantitative description for UGa_2. Further, the method is applied to UFe_{12} and $UFe_{10}Si_2$ ferromagnets. The calculated positive uniaxial magnetic anisotropy together with negative enthalpy of formation for $UFe_{10}Si_2$ make it as a candidate for the magnetically hard materials. Our studies suggest a viable route for further development of the rare-earth-lean permanent magnets by replacing a part of U atoms by some rare-earth like Sm in $UFe_{10}Si_2$.

There is a revival of interest in exploiting the electronic and magnetic character of quantum matter closely connected to unconventional superconductivity with non-trivial topology[1]. Only a handful of quantum materials that show coexistence of ferromagnetism and superconductivity are the uranium-based compounds including UGe_2[2], UTe_2[3], URhGe[4] and UCoGe[5]. The 5*f* electrons in these materials exhibit competing itinerant and localized characteristics between magnetic, and heavy Fermi liquid behaviour.

This itinerant-localized dichotomy is itself not so unusual in metallic actinide compounds, reflecting the "dual" nature[6] often exhibited by open 5*f* shells. Hill recognized the shortest U–U separation as a critical parameter in uranium intermetallics and provided the "Hill plot"[7,8] of magnetic or superconducting ordering temperature versus U–U separation. If shorter than 3.5 Å, the 5*f* states are itinerant and sometimes superconducting, if longer they display a local moment and usually order. This Hill's critical separation is not absolute: it was found to be violated in the heavy fermion metals UPt_3 and UBe_{13} found to be superconducting without magnetic order. Still, the Hill criterion is a very useful and physically motivated guide.

This dual nature of the 5*f* shell requires that both local and itinerant features of the *f*-electrons may need to be allowed in a description of the electronic structure of uranium compounds. Experimentally, they can be examined by photoemission spectroscopy (PES) where the localization would lead to a low density of states (DOS) at the Fermi level (E_F). Experimental PES can be compared to the results of the density functional theory (DFT) calculations in order to examine validity of DFT, and to explain the experimental data in terms of quantitative and material specific electronic band structure[9].

The itinerant-localized dichotomy of the actinides plays not only a fundamental role, but can have important practical implications. In the resent years there is an extensive research targeting new permanent magnets with reduced amount of the rare-earth[10]. A good permanent magnet ought to have reasonably high Curie temperature, a large magnetisation for a high energy product, and a substantial uniaxial magnetic anisotropy to resist demagnetisation[11]. In some of the uranium intermetallics[12] the U-atoms carry large magnetic moments (both spin and orbital), and a huge magnetic anisotropy. Uranium compounds U-(T = 3*d*) with a high content of the transitional metals, in which both U and 3*d* atoms are magnetic, have a potential as magnetically hard materials. Unfortunately, in most of the cases the anisotropy has a multiaxial type (easy-plane)[12]. The only thermodynamically stable U compound with high uniaxial anisotropy, and high Curie temperature of 650 K is $UFe_{10}Si_2$[13], and shares the same $ThMn_{12}$-type tetragonal crystal structure as some of the rare-earth $RE(Fe,Si)_{12}$ compounds[14,15].

Here, we examine the itinerant-localized dichotomy in selected U-based ferromagnets making use of the local-spin-density plus Coulomb-U approach (LSDA+U). At first, we recall the electronic and magnetic character

[1]Institute of Physics, Czech Academy of Sciences, Na Slovance 2, 18221 Prague, Czech Republic. [2]Department of Molecular Chemistry and Materials Science, Weizmann Institute of Science, 76100 Rehovoth, Israel. [3]IT4Innovations and Nanotechnology Centre, CEET, VSB-Technical University of Ostrava, 17. listopadu 2172/15, 70800 Ostrava-Poruba, Czech Republic. [4]Nuclear Engineering Unit, Ben Gurion University of the Negev, 84105 Beer-sheva, Israel. ✉email: shick@fzu.cz

of well-known UGa_2 ferromagnet, and make a comparison between itinerant and localized flavours of LSDA+U. These results are compared with previous experimental and theoretical works and additional features are pointed out. Next, the electronic structure, spin and orbital magnetic moments, and the magnetic anisotropy energy (MAE) for UFe_{12} and $UFe_{10}Si_2$ ferromagnets are presented. We estimate the thermodynamic stability for these materials in terms of the enthalpy of formation, and illustrate that the Si atom substitution into UFe_{12} stabilize the $ThMn_{12}$-type crystal structure. Moreover, it is shown that localized Hubbard-I approximation yields the uniaxial MAE of $UFe_{10}Si_2$ in reasonable agreement with available experimental data. Finally, We suggest that $UFe_{10}Si_2$ ferromagnet is a candidate for magnetically hard material, and predict that $(Sm_{1-x}U_x)Fe_{10}Si_2$ can be a promising candidate for the rare-earth-lean permanent magnet.

Results

The U-atom *f* electrons are mainly responsible for itinerant-localized dichotomy, and the external *spd* electrons make only a discreet contribution to it. Nevertheless, their role can not be disregarded, and we assume that electron interactions in the *s*, *p*, and *d* shells are well approximated in DFT. In this work, the electron correlation effects in 5*f*-manifold are treated making use of two different flavours of local-spin-density plus Coulomb-U approach (LSDA+U): (1) an itinerant orbital polarisation limit (LSDA+U(OP)), and (2) a localized Hubbard-I approximation with the exact atomic limit (LSDA+U(HIA)) described in section "Theoretical methods and computational details". These correlated band theoretical calculations are performed making use of the relativistic version of the full-potential linearized augmented plane wave (FP-LAPW) method including SOC, combined with the rotationally invariant form of LSDA+U implemented as described in Refs.[16,17].

UGa_2. UGa_2 crystallizes in a hexagonal AlB_2 structure[18] (*P6*/*mmm* space group #191). The Ga atoms separate effectively the U atoms, and the shortest U–U interatomic distance of 4.2 Åis well above the Hill limit[7]. This dictates the formation of the local magnetic moments of 2.7[18]–3.0[19] μ_B at the U atoms which are ferromagnetically ordered below the Curie temperature of 125 K.

Experimentally, a large magnetocrystalline anisotropy of − 17 meV/f.u. is found in a single crystal of UGa_2[18] which keeps the magnetization along the [100] direction. The soft-x-ray photoemission (PES) was measured[20] on a single crystal in a ferromagnetic phase well below the Curie temperature. The spectrum shows a narrow peak below the Fermi energy E_F followed by two broader features at 0.5 and 1 eV binding energies, and a hump at about 2.8 eV. Very recently, an unoccupied electron spectrum was investigated by HERFD-XAS[9] in a paramagnetic phase.

Theoretically, there were a few investigations of the electronic structure and magnetic character of UGa_2 ferromagnet[21,22] making use of conventional DFT(LSDA/GGA). These theoretical results[21,22] do not match well the experimental data. Very recently, the electronic and magnetic character of UGa_2 were re-examined[9,23] making use of Wien2k[24] and FPLO[25] codes, and carefully compared with available experimental data. Neither LSDA nor GGA with the SOC included reproduce well experimental value of the magnetization, as it is expected for the materials with narrow 5*f* bands and large orbital magnetic moments.

Different flavours of LSDA+U[23] with Coulomb $U = 1, 2$ eV, and exchange $J = 0.4, 0.6$ eV chosen in the ballpark of commonly asserted values for the uranium intermetallic compounds, as well as GGA plus the orbital polarization correction[26] (GGA+OPC) yield the only partial improvement for the value of the magnetization over DFT results. Also, GGA+OPC reproduce some important features of the experimental PES and XAS spectra, but not to a satisfactory amount.

The magnetic anisotropy energy (MAE) of UGa_2 is investigated in Ref.[23] making use of DFT(LSDA/GGA) and DFT+U. It is evaluated as a difference in the total energes between [100] and [001] magnetization directions, $MAE = E^{[100]} - E^{[001]}$. In contrast to earler LSDA results[21], they report the negative MAE which corresponds to correct [100] easy axis. However the MAE magnitude is substantially smaller than the experimental value[18]. When LSDA+U is applied, the MAE becomes positive, and the [001] easy axis is incorrect, except of the choice for Coulomb $U = 0.8$ eV and unphysicaly small exchange $J = 0.2$ eV values. Simultaneously, the magnetization value is improved over DFT results. The use of spherically symmetric flavour of DFT+U[27] improves the sign of the MAE but worsens the magnetization value. Note that this version of DFT+U is generally not suitable for the uranium-based materials with strong SOC and/or non-collinear magnets[28].

Following a conventional approach, we make use of reduced atomic Hartree–Fock values[29] of the Slater integrals $F_2 = 6.20$ eV, $F_4 = 4.03$ eV, and $F_6 = 2.94$ eV. The resulting values are Hund's $J = 0.51$ eV, and we select a Hubbard U $(= F_0)$ equal to the value of J for LSDA+U(OP) calculations. With this choice of the Coulomb repulsion U equal to the Hund's exchange J, all spherically symmetric terms in the rotationally invariant U, J correction are set to zero.

In Table 1, we show the occupation of the 5f shell n_f, the m_S and m_L in the uranium atom 5f shell, the ratio $-m_L/m_S$, the total magnetic moment in the unit cell for [100] and [001] directions of the magnetization, and the MAE. Our LSDA results are in good agreement with recently reported WIEN2k calculations[23]. The total magnetic moment per the unit cell is significantly smaller than experimentally reported data[18]. The easy magnetization direction [100] is reproduced correctly, but the magnitude of the MAE is about a half of the experimental value. When the LSDA+U(OP) is used, the total magnetic moment values are improved, mainly due to an enhancement of the U 5f-shell orbital moment m_L, but the MAE becomes positive with the wrong [001] easy axis.

Next, we consider the localized 5f-shell model making use of the LSDA+U(HIA) approximation. The Coulomb repulsion $U = 3$ eV is used together with Hund's $J = 0.51$ eV[30]. The results are shown in Table 1. The magnitude of the U 5f-shell orbital moment m_L is strongly enhanced with respect to LSDA and LSDA+U(OP). The total magnetic moment in the unit cell agrees well with the experimental value of 2.7 μ_B[18] obtained from the magnetization measurements, and the U-atom 5f-shell moment of 2.9 μ_B agrees well with the magnetic moment

	dir.	n_f	m_S	m_L	$-\frac{m_L}{m_S}$	m_{tot}	MAE
LSDA	[100]	2.66	− 1.93	2.76	1.47	0.61	
LSDA	[001]	2.66	− 1.98	2.79	1.41	0.55	− 11.90
LSDA+U(OP)	[100]	2.73	− 1.63	3.73	2.29	1.86	
LSDA+U(OP)	[001]	2.73	− 1.60	3.47	2.17	1.69	11.81
LSDA+U(HIA)	[100]	2.71	− 1.83	4.76	2.93	2.71	
LSDA+U(HIA)	[001]	2.75	− 1.83	4.75	2.60	2.70	− 18.98
Exp.					1.9–3.0	3.0 ± 0.1	− 17.1

Table 1. UGa_2—the occupation of the 5f shell n_f, the spin and orbital magnetic moments in the uranium atom 5f shell, m_S and m_L (in μ_B), their ratio $-m_L/m_S$, the total magnetic moment in the unit cell m_{tot} (in μ_B), and the magnetic anisotropy energy MAE (in meV) in comparison with experimental data. The results of LSDA, LSDA+U(OP), and LSDA+U(HIA) for the magnetization constrained along [100] and [001] crystal directions are shown.

of 3.0 ± 0.1 μ_B[19] from polarized neutron scattering data. The negative MAE of − 18.98 meV per unit cell is evaluated in a good quantitative agreement with the experimental value. The minus sign of MAE means that the [100] is the easy magnetization axis in agreement with experimental observation.

In Fig. 1A, we show the total DOS, the U-5f projected DOS and a sum of all non-f DOS for ferromagnetic UGa_2 with the magnetization along the [100] easy direction, in a comparison with the experimental PES[20]. There is a narrow peak in the DOS ≈ 0.1 eV below E_F, in agreement with PES which has the 5f-character. Next to it there is another sharp peak in the DOS at ≈ 0.35 eV binding energy with the 5f-character, and a broader feature between 0.4 and 0.7 eV of the U-6d and Ga-4p non-f character. Experimentally, there are two relatively broad features at 0.5 and 1.0 eV. This inconsistency between the theoretical DOS and the experimental PES comes from a luck of hybridization between Ga-4p and U-5f states in the Hubbard-I approximation. When the exact diagonalization (Lanczos) is used[31] instead, agreement between theory and experiment is somewhat improved.

The unoccupied part of the spectrum can be accessed by an X-ray adsorption spectroscopy making use of a high-energy resolution fluorescence detection mode (HERFD-XAS) at the uranium M_4 edge[9]. In Fig. 1B, the experimental M_4 spectra are compared with the projected $j = 5/2$ U-5f DOS (the experimental spectrum is aligned with the theoretical main peak above the E_F). It is seen that $j = 5/2$ f-DOS is in a reasonable agreement with the experimental data as well as the LSDA+DMFT results[9].

Finally, our calculations indicate that the itinerant LSDA and LSDA+U(OP) treatment of the U 5f-manifold does not provide the consistent description of magnetism in UGa_2. The LSDA+U(HIA) calculations illustrate that the local Hubbard-I model with exact atomic limit for treating 5f-electrons in UGa_2 describes the magnetic, anisotropic and spectroscopic properties better than the conventional DFT or DFT+OPC, in a reasonable quantitative agreement with more sophisticated and computationally demanding LSDA+DMFT[31].

UFe_{12} and $UFe_{10}Si_2$. Next, we turn to salient aspect of our investigation, the magnetic anisotropic properties of UFe_{12} and $UFe_{10}Si_2$. The body-centered tetragonal $ThMn_{12}$-type crystal structure (I4/mmm) is shown in Fig. 2. In the calculations, we use the experimental crystal and internal parameters[32]. The FP-LAPW basis parameters, and values of Slater integrals are chosen as for the case of UGa_2.

The spin m_S and orbital m_L magnetic moments (in μ_B) aligned along [001] crystal direction for U and Fe atoms in different Wyckoff positions, calculated with LSDA+U(HIA) are shown in Table 2. We note the antiparallel alignment of the U and Fe spin m_S magnetic moments in accordance to well established mechanism[33,34] in the rare-earth-Fe intermetallic compounds. Comparison with the results of LSDA+U(OP) (see Table S1 in the Supplemental information) shows that the main difference comes from enhancement of the orbital magnetic moment on the U-atom in LSDA+U(HIA) , while both the spin and orbital moments of the Fe atoms remain almost untouched by the 5*f*-shell Coulomb interactions.

In Fig. 3A, we show the total DOS, the U-5f projected DOS and a sum of all non-f DOS for ferromagnetic UFe_{12} with the magnetization along the [001] easy axis as a result of LSDA+U(HIA) calculations. It is seen that most of the total DOS near E_F does not have the *f*-character, and stems from the Fe atom *d*-states. The *f*-states are located ≈ 0.5 to 1.5 eV below the Fermi edge. On a contrary, in the itinerant LSDA+U(OP) picture the total DOS (see Fig. S1 in the Supplemental information) includes the U-5f DOS contribution at E_F. As it is expected, the *f*-states are substantially more delocalized.

The LSDA+U(OP) yields the strong and negative MAE = − 67.5 meV/f.u., which corresponds to the easy-plane magnetic moment orientation along the [100] axis. The LSDA+U(HIA) calculated MAE = 11.12 meV/f.u. is positive, and is comprised from the U-atom f-shell contribution (8.9 meV), and the Fe contribution of 2.2 meV/f.u. Thus, the localized model predicts the uniaxial MAE for UFe_{12}.

We estimate the structural stability of UFe_{12} calculating the enthalpy of formation ΔH, $\Delta H = E - \sum_i \mu_i x_i$, where E is the LSDA total energy of the UFe_{12}, μ_i is the chemical potential of element i and x_i is the quantity of element i in the compound[35]. The standard convention is to take the chemical potential of each species to be the DFT total energy of the elemental Fe and α-U ground state. The enthalpy of formation is found to be ΔH = 3.349 eV/f.u. The positive sign of ΔH indicates that pristine UFe_{12} is not thermodynamicaly stable.

The available experimental data[13–15] confirm stability of the tetragonal $ThMn_{12}$-type structure for some rare earth and uranium compounds $RFe_{10}Si_2$, when the rare earth or actinide R have an atomic radius smaller than

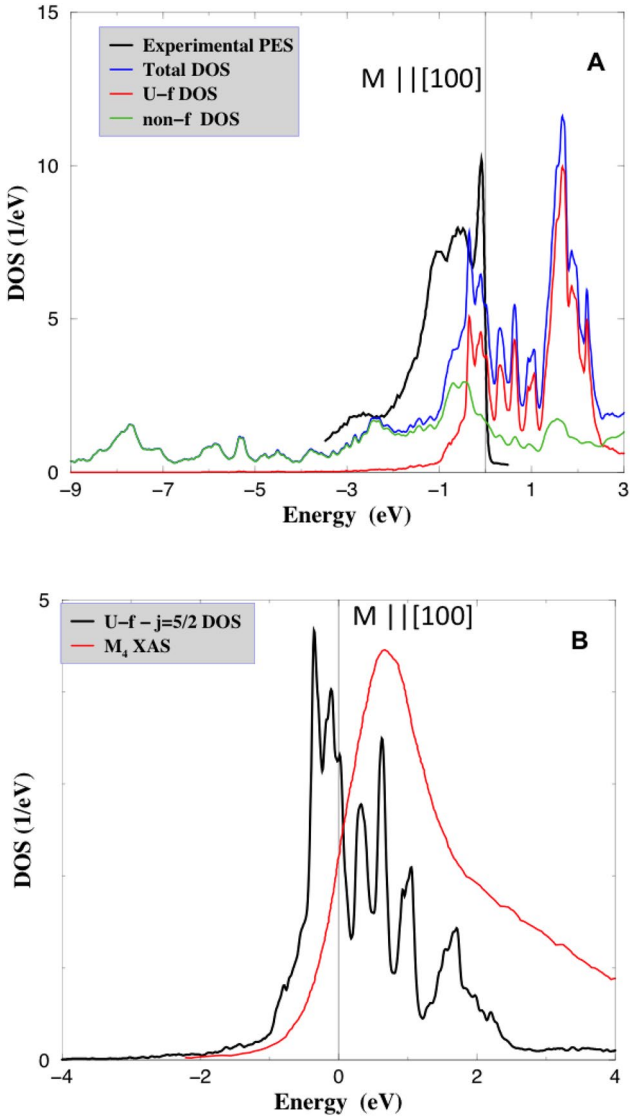

Figure 1. UGa_2—(**A**) Experimental photoelectron spectra (black line) from[20] are compared to the total DOS, orbital-resolved U-5f and a sum of all non-f DOS. (**B**) Experimental HERFD XAS spectra for U-5f (black line) from[9] are compared to the calculated $j = 5/2$-projected U-f DOS. All theoretical DOS correspond to the ferromagnetic solution with [100] magnetic moment alignments.

1.81 Å[36], and Fe is substituted by Si. We consider the effect of Si substitution in $UFe_{10}Si_2$. Experimentally, the Si atoms randomly occupy the (8f) and (8j) Wyckoff positions of the Fe-atoms[13,32] shown in Fig. 2. This inherent disorder can not be modeled in our calculations. In order to discern the electronic structure of $UFe_{10}Si_2$ we assume that Si atoms occupy the (8f) sites only, keep the thirteen atoms unit cell, and preserve the inversion symmetry (see Fig. S2 in the Supplemental information). At first, we estimate the enthalpy of formation ΔH = – 1.425 eV/f.u. in LSDA. Negative sign of ΔH points on the thermodynamic stability of $UFe_{10}Si_2$ upon the Fe atom replacement by Si, in qualitative agreement with available experiment.

We cannot estimate the enthalpy of formation ΔH within the localized LSDA+U(HIA) model since the different total energy functionals are used for UFe_{12} and $UFe_{10}Si_2$ on the one hand, and α-U on the other hand. Nevertheless, we can estimate the change of the enthalpy due to the Fe atom substitution by the Si atom, and have found that $\Delta H(UFe_{10}Si_2) - \Delta H(UFe_{12})$ = – 3.234 eV. It means that the Si substitution tends to thermodynamically stabilise the crystal structure. Note that this comparison has to be taken with some cautiousness since it is done for T = 0 K and without phonon contribution.

The spin m_S and orbital m_L magnetic moments (in μ_B) aligned along [001] crystal direction for U, Si and Fe atoms in different Wyckoff positions, calculated with LSDA+U(HIA) are shown in Table 2. We note that the U-atom spin and orbital magnetic moments are weakly affected by Si substitution. The Si atoms remain almost non-magnetic. While the Fe atoms in (8f) Wyckoff positions keep almost the same spin and orbital magnetic character as in UFe_{12}, the m_S on Fe-(8j), and especially on Fe-(8i) is reduced. The resulting total magnetic moment

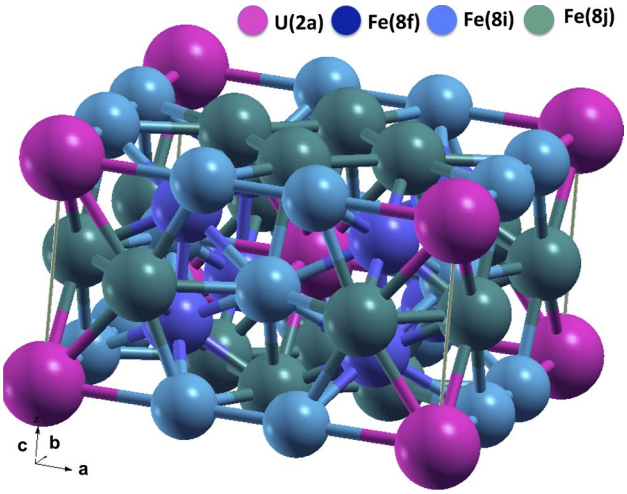

Figure 2. The $ThMn_{12}$-type lattice of UFe_{12} with uranium atoms in 2a Wyckoff position shown in pink, and the Fe atoms in 8f (dark blue), 8j (light blue), and 8i (green) Wyckoff positions. The uranium and iron magnetic moments are aligned along the [001] direction.

Atom	U (2a)		Fe (8f)	Fe (8i)	Fe (8j)	Unit cell
UFe_{12}						
m_S	− 2.28		1.68	2.42	2.05	21.94
m_L	4.57		0.06	0.10	0.09	5.61
m_{tot}	2.29		1.74	2.52	2.14	27.55
U-atom MAE = 8.92 meV				Total MAE = 11.12 meV		
Atom	**U (2a)**	**Si(8f)**	**Fe (8f)**	**Fe (8i)**	**Fe (8j)**	**Unit cell**
$UFe_{10}Si_2$						
m_S	− 2.28	− 0.08	1.69	2.29	1.91	17.25
m_L	4.70	0.00	0.07	0.11	0.11	5.73
m_{tot}	2.42	− 0.08	1.76	2.40	2.02	21.92
U-atom MAE = 2.56 meV				Total MAE = 3.99 meV		
Exp. MAE = 3.1 meV (3 MJ/m^3), m_{tot} = 16.5 μ_B						

Table 2. The spin m_S and orbital m_L magnetic moments (in μ_B) for U and Fe atoms in different Wyckoff positions, aligned along [001] crystal direction. The total magnetic moment in the unit cell m_{tot}, and the magnetic anisotropy energy MAE (in meV) in comparison with experimental data.

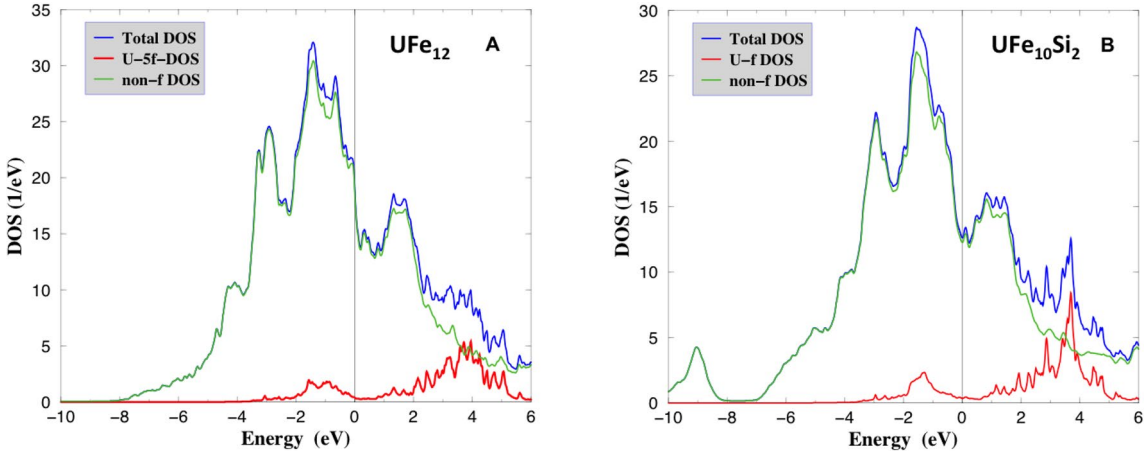

Figure 3. (**A**) The total DOS, orbital-resolved U-5f and a sum of all non-f DOS for UFe_{12}. (**B**) The total DOS, orbital-resolved U-5f and a sum of all non-f DOS for $UFe_{10}Si_2$.

per unit cell of 21.9 μ_B is substantially reduced from the 27.6 μ_B value for UFe_{12}, bringing it somewhat closer to the experimental 16.5 μ_B value.

In Fig. 3B, we show the total DOS, the U-5f projected DOS and a sum of all non-f DOS for ferromagnetic $UFe_{10}Si_2$ with the magnetization along the [001] easy axis as a result of LSDA+U(HIA) calculations. Similar to the case of UFe_{12} (cf. Fig. 3B) most of the total DOS near E_F does not have the *f*-character. Again, the Fe atom *d*-states contribute the most into the total DOS, which is reduced in a comparison with UFe_{12} following a reduction of a number of the Fe atoms. The *f*-states are peaked at ≈ 1.5 eV below the Fermi edge. On a contrary, in the itinerant LSDA+U(OP) picture, the total DOS (see Fig. S1B in the Supplemental information) includes the U-5f DOS contribution at E_F, and the U-5*f*-states are substantially more delocalized in LSDA+U(OP) calculations.

The LSDA+U(HIA) calculated MAE = 4.0 meV/f.u. is positive, and consists of the U-atom single-ion contribution (2.6 meV), and the Fe contribution of 1.4 meV/f.u. Thus, the localized LSDA+U(HIA) model predicts the uniaxial MAE for $UFe_{10}Si_2$ in a reasonable quantitative agreement with the experimental value of 3.1 meV/f.u.[13].

Discussion and summary

To be a good magnet, a ferromagnetic compound should have a Curie temperature, T_c, above 400 K, a saturation moment in a range of 1 MA/m, and the uniaxial magnetic anisotropy of about 4 MJ/m^3[37]. For instance, one of the best permanent magnets, $Nd_2Fe_{14}B$, has a T_c of 588 K, the saturation moment of 1.28 MA/m, and the uniaxial MAE of 4.9 MJ/m^3 with the tetragonal easy *c*-axis[38].

As follows from Table 2 for $UFe_{10}Si_2$, the calculated magnetic moment is of 1.23 MA/m ($\mu_0 M_s = 1.55$ T), and the MAE density, $K_u = 2.41$ MJ/m^3, is somewhat below the standard (≈ 4 MJ/m^3) required for good permanent magnets[11]. The anisotropy field estimated as $H_a = 2K_u/M_s = 3.9$ T which is slightly above the required value of 3.75 T[39]. The maximum energy product $BH_{max} = 1/4\mu_0 {M_s}^2 = 475$ KJ/m^3 is comparable to $BH_{max} \approx 460$ KJ/m^3 in the rare-earth intermetallics $Nd_2Fe_{14}B$[40]. The hardness parameter[41] $k = \sqrt{K_u/\mu_0 {M_s}^2} = 1.13$. Thus, $UFe_{10}Si_2$ can be considered as a candidate to the magnetically hard material. We note that LSDA+U(HIA) calculations (as well as LSDA+U(OP) shown in Supplemental information Table S1) overestimate the total magnetic moment for $UFe_{10}Si_2$ by $\approx 25\%$. Once we take this difference into account, the anisotropy field $H_a = 5.2$ T will be increased, and the energy product $BH_{max} = 267$ KJ/m^3 will be decreased.

The $SmFe_{12}$ family has long been of interest as the rare-earth-lean hard magnetic materials[42]. Replacing the Sm atoms with atomic radius of 1.81 Å by smaller Zr atoms (1.60 Å)[43] leads to stabilisation of $(Sm_{0.7}Zr_{0.3})Fe_{10}Si_2$ alloys into the 1:12 $ThMn_{12}$-type structure[44]. Since the empirical atomic radius of uranium (1.56 Å) is close to Zr, we expect the $(Sm_{1-x}U_x)Fe_{10}Si_2$ alloys to crystallize in 1:12 structure. Moreover, since experimental K_u for $SmFe_{10}Si_2$ is ≈ 7 to 8 MJ/m^3[45], the $(Sm_{1-x}U_x)Fe_{10}Si_2$ alloy is expected to have a higher K_u than $UFe_{10}Si_2$. We note that since the T_c for $UFe_{10}Si_2$ is about 640 K[46], and about 600 K[45] for $SmFe_{10}Si_2$, the $(Sm_{1-x}U_x)Fe_{10}Si_2$ alloy is expected to have reasonably high T_c above 400 K. Since LSDA+U(HIA) can achieve an accurate description of the Sm and U atoms *f*-shell, it can serve in a future investigation of magnetism and magnetic anisotropy in $(Sm_{1-x}U_x)Fe_{10}Si_2$.

It is to note that while values of T_c, M_s, K_u determine the ultimate limits for the permanent magnet, they are necessary but not sufficient. Besides the intrinsic bulk properties it is necessary to have a material in which the microstructure can be controlled to yield high coercivity; this is limited by K_u but depends in a complicated way on the microstructure at the mesoscale. Therefore, while good intrinsic properties are essential, one also seeks a ferromagnet that is readily synthesized and amenable to processing.

In summary, our correlated band theory LSDA+U(HIA) calculations, motivated by the Anderson impurity model suggest that the multiconfigurational aspect of the U 5*f*-shell together with a correct atomic limit need to be taken into account in order to reproduce the anisotropic magnetic and spectroscopic properties of selected U-based ferromagnets. Exploration of the itinerant-delocalised dichotomy in UGa_2 demonstrates that U 5*f*-shell is well localized, and LSDA+U(HIA) calculations reproduce reasonably well the spin, orbital and the total magnetic moments, and the MAE together with occupied and unoccupied electronic structure.

For UFe_{12} and $UFe_{10}Si_2$ ferromagnets we explored the thermodynamic stability in terms of the enthalpy of formation, and found out that the Fe atom substitution by the Si atom tends to stabilise the $ThMn_{12}$-type crystal structure. Furthermore, our LSDA+U(HIA) calculations suggest that $UFe_{10}Si_2$ ferromagnet is close to fulfil criteria for magnetically hard material. These results suggest a viable route for enhancing structural stability and intrinsic hard magnetic properties of $UFe_{10}Si_2$ by replacing a part of U atoms by some rare-earth. We predict that $(Sm_{1-x}U_x)Fe_{10}Si_2$ can be a promising candidate predict that $(Sm_{1-x}U_x)Fe_{10}Si_2$ can be a promising candidate for the magnetically hard material. Our studies can have an important impact on further development of the rare-earth-lean permanent magnets.

Theoretical method and computational details

Theoretical calculations are preformed using the LSDA+U total energy functional in the rotationally invariant form with the spin-orbit coupling (SOC) included[47,48],

$$E^{ee} = \frac{1}{2} \sum_{\gamma_1\gamma_2\gamma_3\gamma_4} n_{\gamma_1\gamma_2} \left(V^{ee}_{\gamma_1\gamma_3;\gamma_2\gamma_4} - V^{ee}_{\gamma_1\gamma_3;\gamma_4\gamma_2} \right) n_{\gamma_3\gamma_4} , \quad (1)$$

which contains the 14×14 on-site occupation matrix $n_{\gamma_1\gamma_2} \equiv n_{m_1\sigma_1,m_2\sigma_2}$ with generally non-zero orbital and spin off-diagonal matrix elements. The V^{ee} is an effective on-site Coulomb interaction, expressed in terms of Slater integrals[16]. The spherically symmetric double-counting energy E^{dc} is subtracted from E^{ee} to correct on the electron-electron interaction already included in DFT. An additional non-spherical double-counting correction is used as described in Ref.[49].

Two flavours of LSDA+U are used. In the first approach, the LSDA+U energy correction $\Delta E^{ee} = E^{ee} - E^{dc}$ can be divided into a sum of spherically symmetric[27] and anisotropic terms. With the artificial choice $U = J$ in Eq. (1), the spherically symmetric part of ΔE^{ee} becomes equal to zero. The remaining anisotropic part of ΔE^{ee} can be regarded as analog of "orbital polarization correction"[26,50] implemented in the LSDA+U language. Therefore, we call it LSDA+U(OP)[51,52], and regard it as an *itinerant model* due to a small value of Coulomb-U which enters the calculations.

In LSDA+U(OP), the MAE is evaluated as a difference in the total energes between [100] and [001] magnetization directions, MAE = $E^{[100]} - E^{[001]}$. Note that the magnetic anisotropy calculation is an involved endeavor, and requires a special care due to a need to insulate small energy differences from a total energy which may be many orders of magnitude larger[53]. The same k-points mesh in the Brillouin zone (BZ) is used in the calculations for both magnetization directions. The special k-points method is used for the BZ integration with the Gaussian smearing of 1 mRy for k-points weighting. The total energy convergence better than 0.01 meV is preserved in the self-consistent LSDA+U(OP) calculations. In order to achieve convergence of the MAE with desired accuracy, about 10,000 k-points are used.

Next is a localized approach[30,54], where it is assumed that the hybridization between the localized *f*-electrons and the itinerant *s*, *p*, and *d*-states is weak, so that the *f*-shell is described with the aid of seven-orbital *f*-shell Anderson impurity model[55] reduced to the atomic limit, also known as the Hubbard-I approximation (HIA)

$$H_{\mathrm{imp}} = \sum_{m\sigma} \varepsilon_f f^{\dagger}_{m\sigma} f_{m\sigma} + \sum_{mm'\sigma\sigma'} \left(\xi \mathbf{l}\cdot\mathbf{s} + \Delta_{\mathrm{CF}} + \frac{\Delta_{\mathrm{EX}}}{2}\hat{\sigma}_z\right)_{m\sigma,m'\sigma'} f^{\dagger}_{m\sigma} f_{m'\sigma'} + \frac{1}{2} \sum_{\substack{mm'm'' \\ m'''\sigma\sigma'}} U_{mm'm''m'''} f^{\dagger}_{m\sigma} f^{\dagger}_{m'\sigma'} f_{m'''\sigma'} f_{m''\sigma}. \tag{2}$$

where $f^{\dagger}_{m\sigma}$ creates an electron in the *f* shell. The parameter ξ specifies the strength of the SOC, Δ_{CF} is the crystal-field potential at the impurity, and Δ_{EX} is the strength of the exchange field. The energy position ε_f ($= -\mu$, the chemical potential) defines the number of *f*-electrons. All of these parameters are calculated self-consistently. The last term describes the Coulomb interactions in the *f*-shell.

The Lanczos method[56] is employed to find the eigenstates of the many-body Hamiltonian H_{imp} Eq. (2) and to calculate the one-particle Green's function $[G_{\mathrm{imp}}(z)]^{\sigma\ \sigma'}_{mm'}$ in the subspace of the *f* orbitals. The self-energy $[\Sigma(z)]^{\sigma\ \sigma'}_{mm'}$ is then obtained from the inverse of the Green's-function matrix $[G_{\mathrm{imp}}]$. Once the self-energy is known, the local Green's function $G(z)$ for the electrons in the solid,

$$[G(z)]_{\gamma_1\gamma_2} = \frac{1}{V_{\mathrm{BZ}}} \int_{\mathrm{BZ}} \mathrm{d}^3\mathrm{k} \left[\mathrm{z} + \mu - \mathrm{H}_{\mathrm{LDA}}(\mathbf{k}) - \Sigma(\mathrm{z})\right]^{-1}_{\gamma_1\gamma_2}, \tag{3}$$

is calculated in a single-site approximation. The local Green's function $G(z)$ is used to evaluate the occupation matrix $n_{\gamma_1\gamma_2} = -\frac{1}{\pi}\ \mathrm{Im} \int_{-\infty}^{E_{\mathrm{F}}} \mathrm{dz}\,[\mathrm{G(z)}]_{\gamma_1\gamma_2}$ in the LSDA+U total energy functional Eq. (1). Note that in this LSDA+U(HIA) approach the atomic limit is explicitly ensured. Interested reader can find the further details of our implementation in Ref.[30].

In LSDA+U(HIA) calculations, we used the two-step procedure to estimate the MAE. At first, we evaluate the U-atom single ion anisotropy making use of recipes of the crystal-field (CF) theory[40]. The CF hamiltonian is constructed from the self-consistent LSDA+U(HIA) results[54,57],

$$\hat{H}_{CF} = \sum_{kq} A^q_k \langle r^k \rangle \Theta_k(J) \hat{O}^q_k\,,$$

where $\hat{O}^q_k$ are the Stevens operator equivalents, $\Theta_k(J)$ are the Stevens factors for a given ground state multiplet *J*, and $A^q_k\langle r^k\rangle$, the crystal field parameters for given *k* and *q*. Next, we follow the CF theory[40], and identify the magnetic anisotropy $E_{MA}(\theta,\phi)$ as a diagonal element $\langle J, J_z = -J|\hat{H}_{CF}|J, J_z = -J\rangle$, where the polar (θ,ϕ) angles specify the magnetization direction. The U atom single-ion contribution in uniaxial MAE $=[E_{MA}(\theta = \pi/2) - E_{MA}(\theta = 0)]$ is calculated.

In order to calculate contribution to the MAE from Fe-sublattice in UFe_{12} and $UFe_{10}Si_2$, we substituted the uranium atom by the yttrium atom, and performed the LSDA calculations. The magnetic force theorem[58] together with the magnetic torque approach[59] were used to evaluate the Fe-sublattice contribution to the uniaxial MAE. This contribution was added to the single-ion U-atom MAE in order to obtain the total anisotropy per unit cell.

Data availability

The data used during the current study available from the corresponding author on reasonable request.

Received: 21 December 2022; Accepted: 10 February 2023
Published online: 14 February 2023

References

1. Sato, M. & Ando, Y. Topological superconductors: A review. *Rep. Prog. Phys.* **80**, 076501 (2017).
2. Saxena, S. *et al.* Superconductivity on the border of itinerant-electron ferromagnetism in UGe_2. *Nature* **406**, 587 (2000).
3. Ran, S. *et al.* Nearly ferromagnetic spin-triplet superconductivity. *Science* **365**, 684 (2019).
4. Aoki, D. *et al.* Coexistence of superconductivity and ferromagnetism in URhGe. *Nature* **413**, 613 (2001).
5. Huy, N. T. *et al.* Superconductivity on the Border of Weak Itinerant Ferromagnetism in UCoGe. *Phys. Rev. Lett.* **99**, 067006 (2007).

6. Zwicknagl, G. 5f electrons in actinides: Dual nature and photoemission spectra. *Int. J. Mod. Phys. B* **21**, 2232 (2007).
7. Hill, H. The early actinides: The periodic system's f electron transition metal series. In *Plutonium 1970 and Other Actinides* (ed. Miner, W. N.) 2 (Metallurgical Society of the AIME, 1970).
8. Boring, A. M. & Smith, J. L. Plutonium condensed matter physics: A survey of theory and experiment. *Los Alamos Sci.* **26**, 90 (2000) (**An updated uranium Hill plot is provided in this publication**).
9. Kolomiets, A. *et al.* 5f states in UGa_2 probed by x-ray spectroscopies. *Phys. Rev. B* **104**, 045119 (2021).
10. Skokov, K. P. & Gutfleisch, O. Heavy rare earth free, free rare earth and rare earth free magnets—vision and reality. *Scr. Mater.* **154**, 289 (2018).
11. Gutfleisch, O. *et al.* Magnetic materials and devices for the 21st century: Stronger, lighter, and more energy efficient. *Adv. Mater.* **23**, 821 (2011).
12. Andreev, A. *et al.* Magnetic anisotropy in intermetallic compounds containing both uranium and 3d-metal. *Phys. Met. Metallogr.* **114**, 727 (2013).
13. Andreev, A., Bartashevich, M., Katori, H. A. & Goto, T. Magnetic anisotropy and magnetostriction of $UFe_{10}Si_2$. *J. Alloys Compd.* **216**, 221 (1995).
14. Buschow, K. Structure and properties of some novel ternary Fe-rich rare-earth intermetallics. *J. Appl. Phys.* **63**, 3130 (1988).
15. Ohashi, K., Tawara, Y., Osugi, R. & Shimao, M. Magnetic properties of Fe-rich rare-earth intermetallic compounds with a $ThMn_{12}$ structure. *J. Appl. Phys.* **64**, 7514 (1988).
16. Shick, A. B., Liechtenstein, A. I. & Pickett, W. E. Implementation of the LDA+U method using the full-potential linearized augmented plane-wave basis. *Phys. Rev. B* **60**, 10763 (1999).
17. Shick, A. B., Janis, V., Drchal, V. & Pickett, W. E. Spin and orbital magnetic state of UGe_2 under pressure. *Phys. Rev. B* **70**, 134506 (2004).
18. Andreev, A. *et al.* Crystal structure, and magnetic and magnetoelastic properties of UGa_2. *J. Exp. Theor. Phys.* **48**, 1187 (1978).
19. Lawson, A. *et al.* Magnetic neutron diffraction study of UGa_3 and UGa_2. *J. Magn. Magn. Mater* **50**, 83 (1985).
20. Fujimori, S.-I. *et al.* Manifestation of electron correlation effect in 5f states of uranium compounds revealed by $4d-5f$ resonant photoelectron spectroscopy. *Phys. Rev. B* **99**, 035109 (2019).
21. Divis, M., Richter, M., Eschrig, H. & Steinbeck, L. Ab initio electronic structure, magnetism, and magnetocrystalline anisotropy of UGa_2. *Phys. Rev. B* **53**, 9658 (1996).
22. Honma, T. *et al.* Magnetic and fermi surface properties of the ferromagnetic compound UGa_2. *J. Phys. Soc. Jpn.* **69**, 2647 (2000).
23. Chatterjee, B. & Kolorenc, J. Magnetism and magnetic anisotropy in UGa_2. *MRS Adv.* **5**, 2639 (2020).
24. Blaha, P. *et al.* WIEN2k: An APW+lo program for calculating the properties of solids. *J. Chem. Phys.* **152**, 074101 (2020).
25. Koepernik, K. & Eschrig, H. Full-potential nonorthogonal local-orbital minimum-basis band-structure scheme. *Phys. Rev. B* **59**, 1743 (1999).
26. Eriksson, O., Johansson, B. & Brooks, M. S. S. Meta-magnetism in UCoAl. *J. Phys. Condens. Matter* **1**, 4005 (1989).
27. Dudarev, S. L., Botton, G. A., Savrasov, S. Y., Humphreys, C. J. & Sutton, A. P. Electron-energy-loss spectra and the structural stability of nickel oxide: An LSDA+U study. *Phys. Rev. B* **57**, 1505 (1998).
28. Dudarev, S. *et al.* Parametrization of LSDA+U for noncollinear magnetic configurations: Multipolar magnetism in UO_2. *Phys. Rev. Mater.* **3**, 083802 (2019).
29. Moore, K. T. & van der Laan, G. Nature of the 5f states in actinide metals. *Rev. Mod. Phys.* **81**, 235 (2009).
30. Shick, A. B., Fujimori, S.-I. & Pickett, W. E. UTe_2: A nearly insulating half-filled $j=\frac{5}{2}, 5f^3$ heavy fermion metal. *Phys. Rev. B* **103**, 125136 (2021).
31. Chatterjee, B. & Kolorenc, J. Electronic structure and magnetism in UGa_2: DFT+DMFT approach. *Phys. Rev. B* **103**, 205146 (2021).
32. Berlureau, T., Chevalier, B., Gravereau, P., Fournes, L. & Etourneau, J. Investigation of the $U(Fe_{10-x}Co_x)Si_2$ ternary system with $0 \geq x \leq 10$ by X-ray powder diffraction, magnetic and 57Fe Mossbauer studies. *J. Magn. Magn. Mater* **102**, 166 (1991).
33. Brooks, M., Eriksson, O. & Johansson, B. 3d–5d band magnetism in rare earth transition metal intermetallics: $LuFe_2$. *J. Phys. Condens. Matter* **1**, 5861 (1989).
34. Campbell, I. Indirect exchange for rare earths in metals. *J. Phys. F* **2**, L47 (1972).
35. Kyvala, L., Tchaplianka, M., Shick, A. B., Khmelevskyi, S. & Legut, D. Large uniaxial magnetic anisotropy of hexagonal Fe–Hf–Sb alloys. *Crystals* **10**, 430 (2020).
36. Sakurada, S., Tsutai, A. & Sahashi, M. A study on the formation of $ThMn_{12}$ and $NaZn_{13}$ structures in $RFe_{10}Si_2$. *J. Alloys Compd.* **187**, 67 (1992).
37. Skomski, R. & Coey, J. M. D. *Permanent Magnetism* (CRC Press, 1999).
38. Givord, D., Li, H. & De La Bathie, R. P. Magnetic properties of $Y_2Fe_{14}B$ and $Nd2Fe_{14}B$ single crystals. *Solid State Commun.* **51**, 857 (1984).
39. Landa, A., Soderlind, P., Moore, E. E. & Perron, A. Thermodynamics and magnetism of $SmFe_{12}$ compound doped with Co and Ni: An ab initio study. *Appl. Sci.* **12**, 4860 (2022).
40. Herbst, J. F. $R_2Fe_{14}B$ materials: Intrinsic properties and technological aspects. *Rev. Mod. Phys.* **63**, 819 (1991).
41. Skomski, R. & Coey, J. Magnetic anisotropy—how much is enough for a permanent magnet?. *Scr. Mater.* **112**, 3 (2016).
42. Buschow, K. Permanent magnet materials based on tetragonal rare earth compounds of the type $RFe_{12-x}M_x$. *J. Magn. Magn. Mater* **100**, 79 (1991).
43. Earnshaw, A. & Greenwood, N. N. *Chemistry of the Elements* Vol. 60 (Butterworth-Heinemann Oxford, 1997).
44. Gabay, A., Shchegoleva, N. & Belozerov, E. The structure and hard magnetic properties of rapidly quenched (Sm, Zr)(1)(Fe, Si)(12) alloys. *Phys. Met. Metallogr.* **94**, 252 (2002).
45. Solzi, M., Xue, R. H. & Pareti, L. Magnetic anisotropy and first-order magnetization processes in $Sm(Fe_{1-x}Co_x)_{10}M_2$ (M = Ti, Si) compounds. *J. Magn. Magn. Matter* **88**, 44 (1990).
46. Waerenborgh, J. C., Rogalski, M. S., Gonsalves, A. P., Sousa, J. B. & Almeida, M. Mossbauer spectroscopy study of 3d-magnetic properties in $UFe_{10}Si_2$. *Solid State Commun.* **104**, 271 (1997).
47. Solovyev, I., Liechtenstein, A. & Terakura, K. Is Hund's second rule responsible for the orbital magnetism in solids?. *Phys. Rev. Lett.* **80**, 5758 (1998).
48. Savrasov, S. Y. & Kotliar, G. Ground state theory of δ-Pu. *Phys. Rev. Lett.* **84**, 3670 (2000).
49. Kristanovski, O., Shick, A. B., Lechermann, F. & Lichtenstein, A. I. Role of nonspherical double counting in DFT+DMFT: Total energy and structural optimization of pnictide superconductors. *Phys. Rev. B* **97**, 201116 (2018).
50. Eschrig, H., Sargolzaei, M., Koepernik, K. & Richter, M. Orbital polarization in the Kohn–Sham–Dirac theory. *EPL* **72**, 611 (2005).
51. Shick, A. B. & Pickett, W. E. Spin–orbit coupling induced degeneracy in the anisotropic unconventional superconductor UTe_2. *Phys. Rev. B* **100**, 134502 (2019).
52. Kyvala, L., Havela, L., Kadzielawa, A. P. & Legut, D. Electrons and phonons in uranium hydrides—effects of polar bonding. *J. Nucl. Mater.* **567**, 153817 (2022).
53. Trygg, J., Johansson, B., Eriksson, O. & Wills, J. M. Total energy calculation of the magnetocrystalline anisotropy energy in the ferromagnetic 3d metals. *Phys. Rev. Lett.* **75**, 2871 (1995).
54. Shick, A. B. & Maca, F. Electronic structure and magnetic properties of Dy-doped Bi_2Te_3. *J. Alloys Compd.* **872**, 159709 (2021).
55. Hewson, A. C. *The Kondo Problem to Heavy Fermions, Cambridge Studies in Magnetism* Vol. 2 (Cambridge University Press, 1993).

56. Kolorenc, J., Poteryaev, A. I. & Lichtenstein, A. I. Valence-band satellite in ferromagnetic nickel: LDA+DMFT study with exact diagonalization. *Phys. Rev. B* **85**, 235136 (2012).
57. Shick, A. B. & Denisov, A. Y. Magnetism of 4f-atoms adsorbed on metal and Graphene substrates. *J. Magn. Magn. Mater* **475**, 211 (2018).
58. Liechtenstein, A. I., Katsnelson, M., Antropov, V. & Gubanov, V. Local spin density functional approach to the theory of exchange interactions in ferromagnetic metals and alloys. *J. Magn. Magn. Mater* **67**, 65 (1987).
59. Khmelevskyi, S., Shick, A. B. & Mohn, P. Element-specific analysis of the magnetic anisotropy in Mn-based antiferromagnetic alloys from first principles. *Phys. Rev. B* **83**, 224419 (2011).

Acknowledgements

We acknowledges partial support provided by Operational Programme Research, Development and Education financed by European Structural and Investment Funds and the Czech Ministry of Education, Youth, and Sports (Project No. SOLID21-CZ.02.1.01/0.0/0.0/16–019/0000760), and by the Czech Science Foundation (GACR) Grant No. 22-22322S. ABS acknowledges financial support from the Israeli Ministry of Aliyah and Integration Grant Ref.:140636. DL acknowledges the project e-INFRA CZ (ID:90140) by the Ministry of Education, Youth and Sports of the Czech Republic.

Author contributions

A.B.S., I.H. and D.L. conceived and supervised the project. A.B.S., M.T., and D.L. performed the computations. All authors contributed to the interpretation of the data and to the writing of the manuscript.

Competing interests

The authors declare no competing interests.

Additional information

Supplementary Information The online version contains supplementary material available at https://doi.org/10.1038/s41598-023-29823-2.

Correspondence and requests for materials should be addressed to A.B.S.

Reprints and permissions information is available at www.nature.com/reprints.

Publisher's note Springer Nature remains neutral with regard to jurisdictional claims in published maps and institutional affiliations.